Supplementary Information for

Candidate electro-optic molecular crystals for future optoelectronic integration

Keishi Sunami[1], Sachio Horiuchi[1], Yoriko Sonoda[1], Naomi Fujiki[1], Toshiki Higashino[1], Yuki Atsumi[2], Shoji Ishibashi[1], and Jun'ya Tsutsumi[1]*

[1]*Core Electronics Technology Research Institute (CETRI), National Institute of Advanced Industrial Science and Technology (AIST), Tsukuba, Ibaraki 305-8565 Japan*
[2]*Photonics-Electronics Integration Research Center (PEIRC), National Institute of Advanced Industrial Science and Technology (AIST), Tsukuba, Ibaraki 305-8568 Japan*

*Corresponding author: k.sunami@aist.go.jp (K.S.), junya.tsutsumi@aist.go.jp (J.T.)

Supplementary Text 1. Second Harmonic Generation (SHG) Measurements. The Kurtz and Perry powder test [S1] was performed at a fundamental wavelength λ = 1.064 μm with the optical path length of 200 μm by measuring the transmitted SHG efficiency relative to urea. The crystals were crushed simply by pushing the wrapping paper sandwiching them and were filtered out to obtain the microcrystalline with particle size of around 63-150 μm. The powdered crystalline croconic acid having the approximate efficiency of 47 times that of urea was repeatedly examined also for regular checking the apparatus with finding the standard deviation of ~30 % on average of 14 specimens.

The observed SHG efficiencies of purified powders relative to urea are NDPA (7.1), PNPA (5.8), OH1 (9.7), CPNC (5.0), DMACB (33, 0.12; before and after melting-re-solidification, respectively), NPRO (110), BNA (250), MNA (700). Note that the NDPA, PNPA, OH1, and CPNC absorb the SH light at $\lambda/2$ = 532 nm, as shown by Fig. S3.

Supplementary Figure 1. Molecular structures of the molecular crystals listed in Fig. 1b but not shown in Fig. 2.

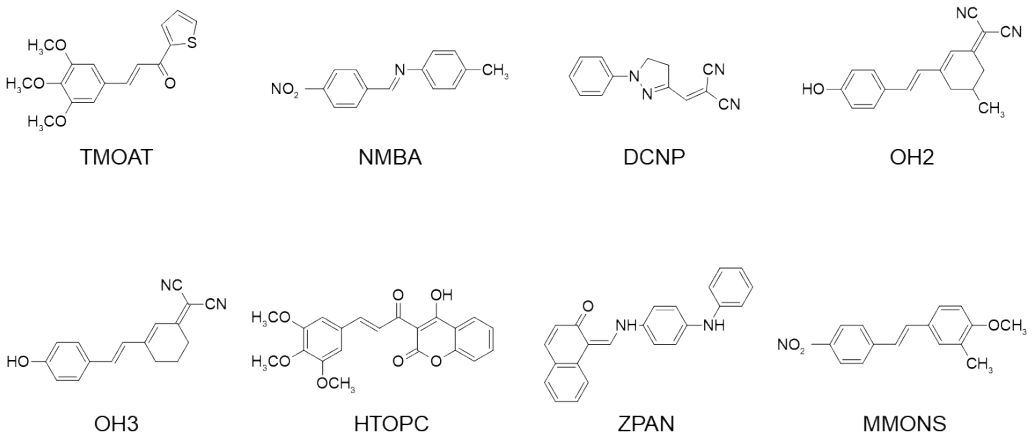

Supplementary Figure 2. Differential scanning calorimetry (DSC) thermographs. Arrows indicate the directions of temperature changes at a rate of 5 K min^{-1}. The inset to panel (f) shows that the phase transition observed before melting disappears below T_m in the second heating runs, suggesting a formation of unknown polymorph after re-solidification. This observation is consistent with the SHG activity being lost with this treatment.

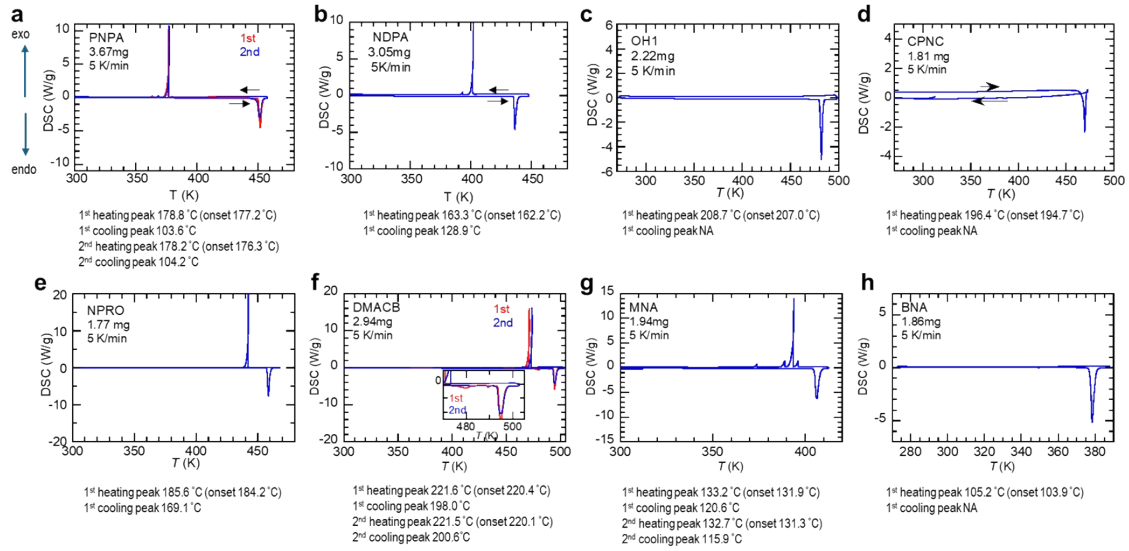

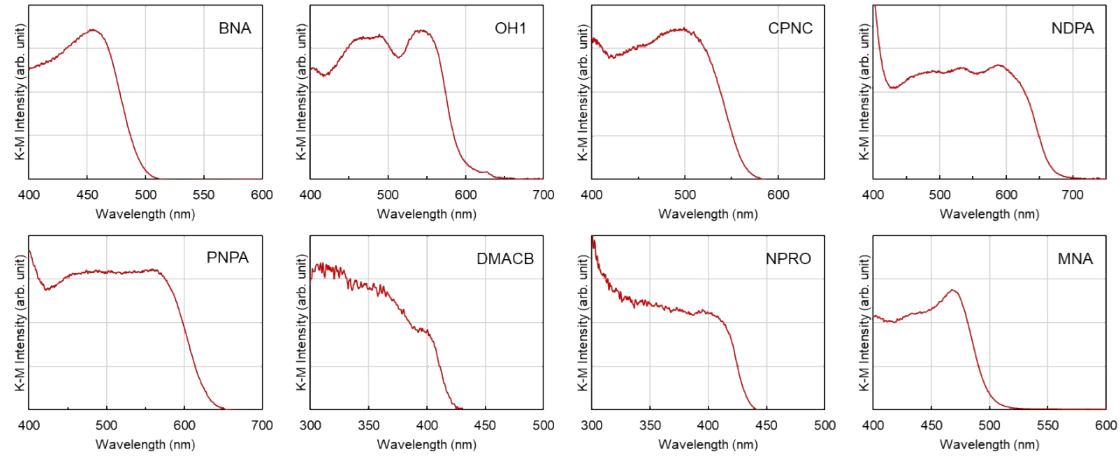

Supplementary Figure 3. Kubelka-Munk (K-M) absorption spectra.

Supplementary Figure 4. Polarized microscope images for PNPA and NDPA thin films. Crossed-Nicols and polarized microscope images for PNPA (upper panels) and NDPA (lower panels) pictured in the transmission setup. The angle between the polarizer (set before the thin film) and the [001] direction (|| *c*) is described at the bottom.

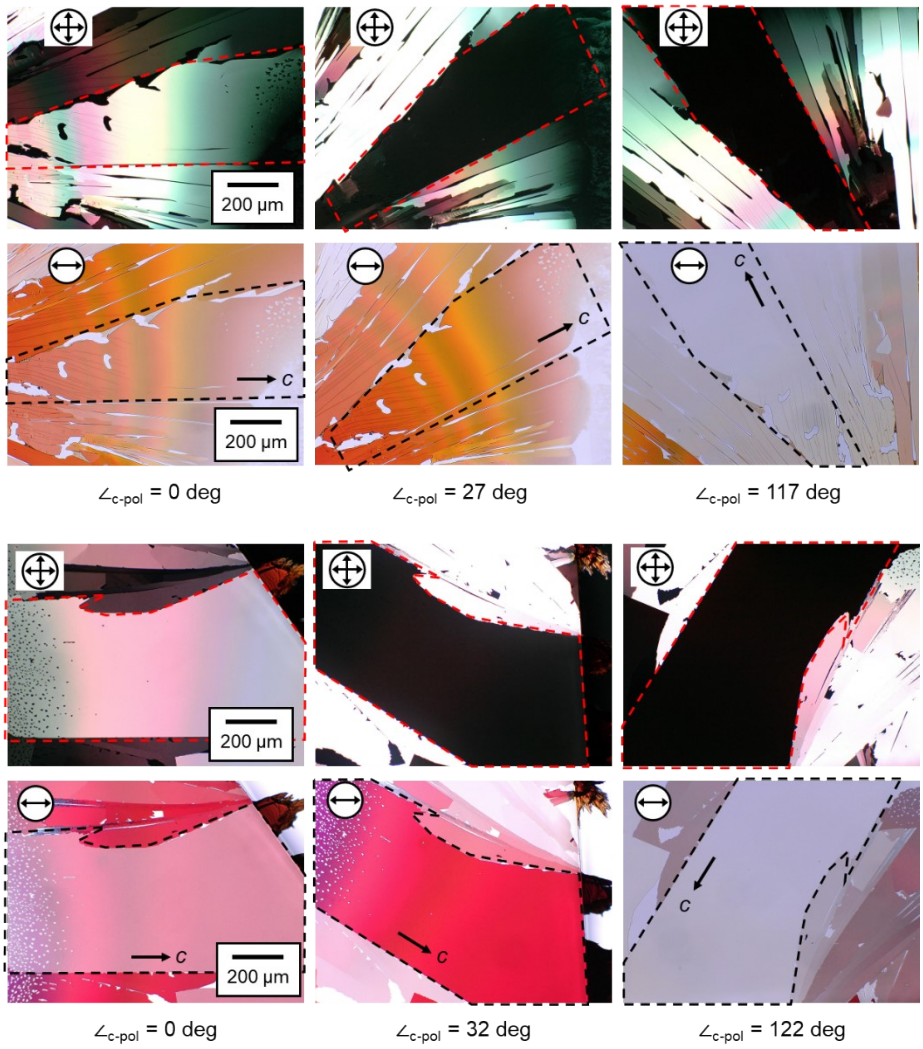

Supplementary Text 2. Determination of the direction of polarity in EO thin films. According to the crystal structure analysis, the polar axis of PNPA is parallel to the [102] direction, which is inclined by about 30 degrees relative to the [001] direction (corresponding the crystal growth axis). Because a strong absorption band due to intramolecular transition at approximately 500 nm exists along the polar axis in PNPA (Table 1), the polarized microscope image appears to be orange-red colored when the polarizer is parallel to the polar axis of EO films. Additionally, the crossed-Nicols image becomes completely dark at a similar angle because the polar axis is

expected to be the dielectric principal axis. The obtained PNPA single crystalline film by the melt casting exhibits these features when the angle between the polarizer and the [001] axis is about 27 degrees (surrounded by the broken line in Fig. S4), indicating the exposure surface plane of the (010) plane with the in-plane polar axis. For NDPA, we observed the similar behaviors at the angle between the polarizer and the [001] axis of 32 degrees, also indicative of the (010) surface film.

Supplementary Figure. 5. Device fabrication process flow for the silicon slot-waveguide structure.

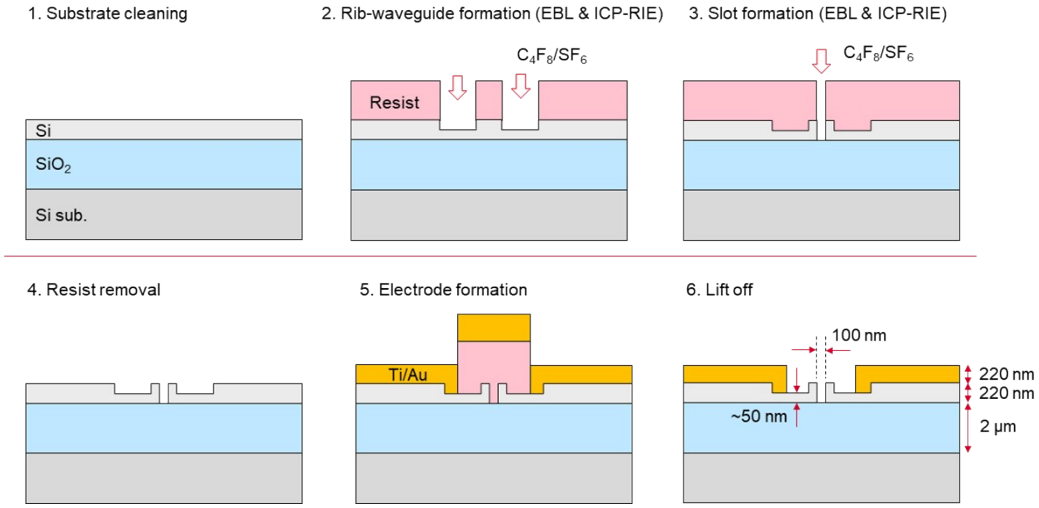

Supplementary Figure. 6. Optical-microscope (left) and SEM (middle and right) images of the silicon slot-waveguide structure.

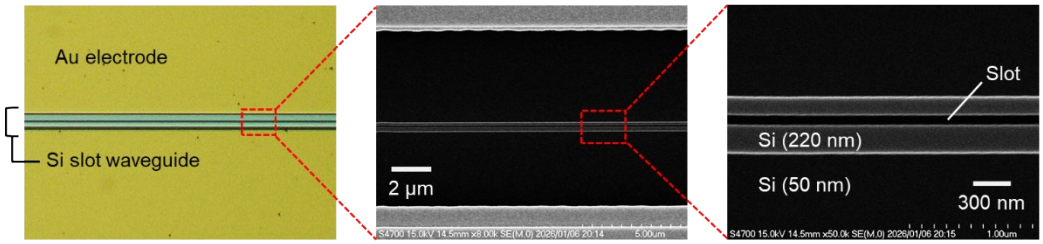

Supplementary Figure 7. Setup for modulation imaging. The EO thin film is positioned such that the polar axis is oriented at 45 degrees relative to the polarizer in the crossed-Nicols configuration.

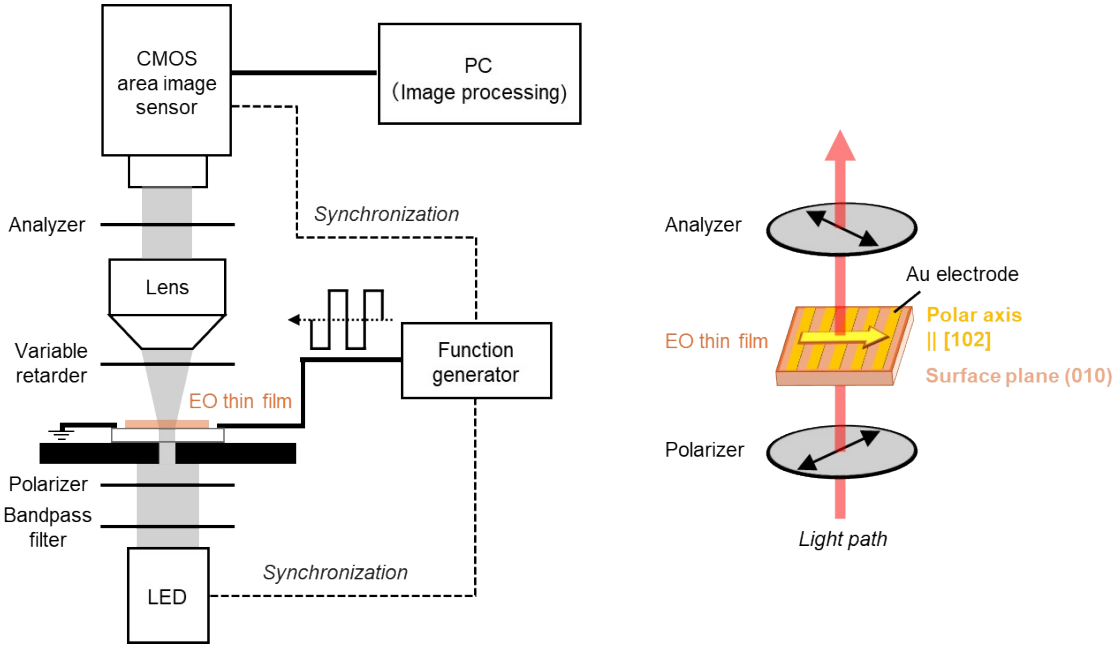

Supplementary Figure 8. Long-term thermal stability tests of PNPA thin film with and without sealing. Crossed-Nicols ($I_\perp$) and modulation ($\Delta I_\perp/I_\perp$) images for PNPA thin film fabricated on the interdigitated electrode substrate, obtained by the FFMI measurements at λ = 810 nm (the displayed images represent a part of the entire measurement area). For the sealed condition, the film was covered with a glass plate. The FFMI measurements were conducted under the phase retardation derived from the variable retarder φ_{ext} of ~180 and ~90 degrees for the sealed and unsealed measurements, respectively. These values were selected to clearly detect the $\Delta I_\perp/I_\perp$ signals in each setup. The φ_{ext} values that maximize $I_\perp$ and $\Delta I_\perp/I_\perp$ differ by ~π,[S2] leading to a dark $I_\perp$ image under the condition optimized for observing the $\Delta I_\perp/I_\perp$ signal.

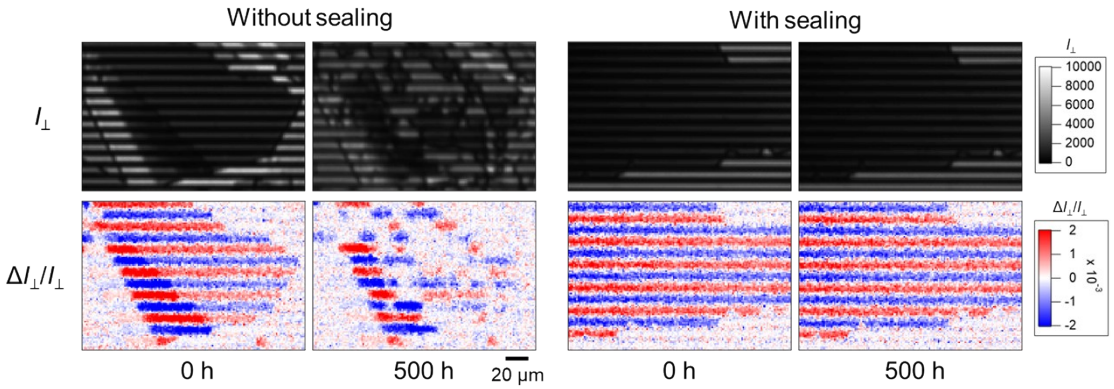

Supplementary references

[S1] S. K. Kurtz and T. T. Perry, *J. Appl. Phys.* **1968**, *39*, 3798.

[S2] K. Sunami, S. Horiuchi, S. Ishibashi, J. Tsutsumi, *Adv. Electron. Mater.* **2025**, *11*, 2400346.